Hindawi
Mathematical Problems in Engineering
Volume 2024, Article ID 9266585, 7 pages
https://doi.org/10.1155/2024/9266585

*Research Article*

# Image Edge Detection by Global Thresholding Using Riemann–Liouville Fractional Integral Operator

**S. Gaur**,[1] **A. M. Khan**,[2] **D. L. Suthar**,[3] **and Avnish Bora**[1]

[1]*Department of Electronics and Communication, JIET Group of Institutions, Jodhpur, India*
[2]*Department of Mathematics, JIET Group of Institutions, Jodhpur, India*
[3]*Department of Mathematics, Wollo University, P.O. Box 1145, Amhara Region, Ethiopia*

Correspondence should be addressed to D. L. Suthar; dlsuthar@gmail.com

Received 11 January 2023; Revised 10 October 2023; Accepted 9 December 2023; Published 19 March 2024

Academic Editor: Toqeer Mahmood



It is difficult to give a fractional global threshold (FGT) that works well on all images as the image contents are totally different. This paper describes an interesting use of fractional calculus in the field of digital image processing. In the proposed method, the fractional global threshold-based edge detector (FGTED) is established using the Riemann–Liouville fractional integral operator. FGTED is used to find the microedges in minimum time for any input digital images. The results demonstrate that the FGTED outperforms conventional techniques for detecting microtype edges. The image with a higher entropy was produced by the FGT value-based approach. Tables and images are used to summarize the output performance analysis of various images using structural similarity index measure, *F*-score (*F*-measure), precision and recall, signal-to-noise ratio, peak signal-to-noise ratio, and computational time. The FGTED can be used to detect very thin or microtype edges more accurately in minimum time without training or prior knowledge.

## 1. Introduction

Fractional calculus is concerned with the mathematical investigation and application of integrals and derivatives of arbitrary order [1]. Given the usefulness and significance of fractional calculus in the analysis of real-world problems, the properties and applications of a variety of fractional integral operators have been studied by a large number of researchers such as McBride [2], Kilbas and Sebastian [3], Kiryakova [4], Baleanu et al. [5], Gaur Sanjay et al. [6, 7], etc. It has been recently found that the application of fractional calculus can be useful for image processing, particularly to enhance the quality of edge detection for the images [8–10]. Edge detection is one of the fundamental tasks in digital image processing. It plays a prominent role in image analysis, pattern recognition, and other deep-level processing [11, 12].

Edges are a collection of pixels where the intensity of each pixel fluctuates dramatically [13]. To identify, segment and recognize an item in an image, edge detection is a very useful and difficult job in computer vision. It is also used in a system for feature identification, compression, and picture retrieval [14–16]. The process of edge detection consists of four main steps: localization, detection, enhancement, and smoothing. The quality of edges diminishes in noisy environments and, in certain cases, after the noise has been suppressed, blurring the image's major transitions. Edge detection necessitates some sort of smoothing since it relies on differentiating the image function, which amplifies all high-frequency components. Low pass filters are the most commonly employed for this [15].

During the last four decades, the topic of fractional calculus, which deals with the study of arbitrary order integrals and derivatives, has grown in relevance and interest. It is mostly owing to its wide range of possible applications in science, engineering, and technology. Various authors have investigated various expansions of several fractional integration operators and their applications in recent years.

Pu et al. [17] investigated a fractional differential approach to the digital processing field for enhancement. The authors have proposed six fractional multiscale differential masks for the enhancement of images. Traditional integral differential-based algorithms perform worse than the suggested fractional differential-based method. They discovered it to be ideal for real-time HDTV, legibility of subsequent bionic medical images (for example, X images, cell pictures, mammography, PET, MRI, CT, and plutonic images), improved bank ticket quality, and improving remote sensing image, among other applications.

For the numerical solution of fractional differential equations, Diethelm et al. [18] described an Adams-type predictor–corrector approach. They have analyzed the results for both linear and nonlinear problems. Finally, it was recommended that their approach can be extended to multiterm equations using more than one differential operator.

Sarikaya and Yaldiz [19] developed a novel Hermite–Hadamard type fractional integral inequalities utilizing a wide class of fractional integral operators. They also applied fractional integral inequalities to develop inequalities of the Hermite–Hadamard type, employing the well-known Riemann–Liouville fractional integral (RLFI) operators.

Ntouyas et al. [20] studied Polya–Szego type integral inequalities using the RLFI operator and utilized them to show various Chebyshev-type fractional integral inequalities affecting the integral of the product of two functions and the product of two integrals. Khmag et al. [21], Khmag [22], and Khmag and Kamarudin [23] studied clustering-based natural image denoising using a dictionary learning approach in the wavelet domain and semisoft thresholding approach and natural image deblurring using a neural network.

Martin et al. [24] have proposed a Berkeley Segmentation Dataset 500 (BSDS500), which is regarded as the standard benchmark for the detection of the edges. Initially, the given database was designed for investigating natural edge detection, which includes object contours, its interior, and boundaries. This dataset includes five hundred natural-type images with regressive annotated boundaries collected from different users. The abovementioned dataset is used in this paper to compare the performance of the fractional global threshold-based edge detector (FGTED) method with the existing prevailed edge detectors.

The Riemann–Liouville fractional calculus integral operator as left-sided fractional integrals is explained in Section 2.

## 2. RLFI Operator

The fractional order integral operators are efficient tools to describe the complex phenomenon in much better ways due to their nonlocal nature and having a tendency to preserve hereditary properties related to the image. Since the gray-level values have a high correlation with the neighboring pixels so the fractional order operators are more efficient to describe the hereditary relation and give better neighboring gray-level information. There are several forms of the fractional integrals for a continuous function *f(t)* have been given by various authors [25]. One of which, known as the Riemann–Liouville fractional calculus operator, has been studied extensively for applications in the area of image processing [8–11].

Further, the left-sided Riemann–Liouville fractional calculus operator, defined by Kilbas et al. [1] for $\varsigma \in C, \Re(\varsigma) > 0$, is applied as follows:

$$\left(I_{0+}^{\varsigma} f\right)(x) = \frac{1}{\Gamma(\varsigma)} \int_0^x \frac{f(t)}{(x-t)^{1-\varsigma}} dt \ (x>0, \Re(\varsigma)>0), \tag{1}$$

where $\Gamma\ (\varsigma)$ is the Gamma function, the above integrals are called *left-sided fractional integrals*. When $\varsigma = n\ N$, Equation (1) can be solved by the well-known $n$th integral formula by Cauchy as given below:

$$\begin{aligned} \int_0^x dt_1 \int_0^{x_1} dt_2 \ldots \int_0^{x_{n-1}} f(t_n) dt_1 &= \frac{1}{(n-1)!} \int_0^x (x-t)^{\varsigma-1} f(t) dt, n \in N \\ &= \frac{1}{\Gamma(\varsigma)} \int_0^x \frac{f(t)}{(x-t)^{1-\varsigma}} dt, n \in N. \end{aligned} \tag{2}$$

Riemann–Liouville fractional integration of the power functions $(t-a)^{\rho-1}$, $\Re\ (\rho) > 0$ is then used to generate power functions of the same form, as given below:

$$\left(I_{a+}^{\varsigma} (x-a)^{\rho-1}\right)(t) = \frac{\Gamma(\rho)}{\Gamma(\rho+\varsigma)} (t-a)^{\rho+\varsigma-1} (\Re(\alpha)>0). \tag{3}$$

This paper emphasizes upon the need to detect the edge in digital images by introducing a fractional global threshold (FGT) value. Further, the investigation demonstrated an interesting application of the RLFI operator [1] for edge detection in image processing. The edge detection based on noninteger integration of the general statistical average improves the detection selectivity of an edge detector.

## 3. Edge Detection by Global Thresholding

The proposed methodology for edge detection consists of three steps: preprocessing and normalization of an image, computation of global threshold by RLFI operator, binarisation, and removal of isolated pixels. A block diagram of the working is shown in Figure 1.

After the camera captures the image (Input Image), it is routed via the preprocessing unit, which processes the raw image. Preprocessing focuses on two fundamental operations: grayscale conversion and contrast stretching, which allows the system to perform consistently well for all images.

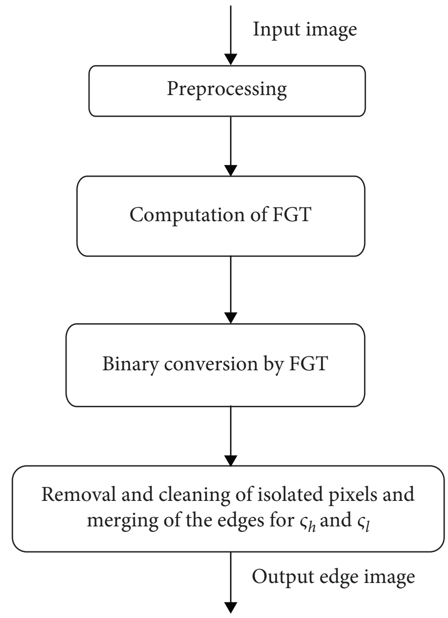


Figure 1: Block diagram of FGTED.

Furthermore, the edge identification procedure is aided if the RGB color input picture is transformed to a 256 grayscale image using the YIQ color space used by the NTSC color system [5], as shown in the following equation:

$$P(i,j) = 0.299\, R(i,j) + 0.587\, G(i,j) + 0.114\, B(i.j). \tag{4}$$

Here $R(i, j)$, $G(i, j)$, and $B(i, j)$ are the red, green, and blue intensities of the $(i, j)$th pixel of the color image, respectively.

In the next step, the filtered image $P(i, j)$ is normalized in the range 0–1 using the following equation:

$$t(i,j) = \frac{P(i,j)}{\mathrm{Max}(P(i,j))}. \tag{5}$$

Further, the left-sided Riemann–Liouville fractional calculus operator for a continuous function $f(x)$ is defined by Kilbas et al. [1] for $\varsigma \in \mathbb{C}$, $\Re(\varsigma) > 0$ is applied as follows:

$$\left(I_{0+}^{\varsigma} f\right)(t) = \frac{1}{\Gamma(\varsigma)} \int_0^t \frac{f(x)}{(t-x)^{1-\varsigma}}\, dx \ (t>0). \tag{6}$$

Riemann–Liouville fractional integration of the power function $(x - a)\rho - 1$, $(\rho) > 0$ is then used to generate power functions of the same form as given below:

$$\left(I_{a+}^{\varsigma}(t-a)^{\rho-1}\right)(x) = \frac{\Gamma(\rho)}{\Gamma(\rho+\varsigma)}(x-a)^{\rho+\varsigma-1}, \ (\Re(\varsigma)>0). \tag{7}$$

Now, if $f(t)$ represents the general statistical average, then by virtue of Equation (6), it can be written as follows:

$$\left(I_{0+}^{\varsigma} f\right)(t) = \frac{1}{\Gamma(\varsigma+2)} \frac{1}{N} \sum_{k=0}^{N} t_k^{\varsigma+1}, \ (\Re(\varsigma)>0). \tag{8}$$

The result of Equation (8) is applied to evaluate FGT for image $t(i, j)$ as follows:

$$\mathrm{FGT} = \frac{1}{\Gamma(\varsigma+2)} \frac{1}{m\times n} \sum_{i=0}^{m} \sum_{j=0}^{n} t^{\varsigma+1}(i,j), \ \text{for } (0<\varsigma\le 1). \tag{9}$$

Now, the FGT is used to convert normalized $t(i, j)$ into binary image $b(i, j)$ with the help of computed FGT as follows:

$$b(i,j) = \begin{cases} 1, & t(i,j) \ge \mathrm{FGT} \\ 0, & t(i,j) < \mathrm{FGT} \end{cases}. \tag{10}$$

Now Algorithm 1 removes the unwanted pixels, leaving only boundary pixels, and cleans the uncoordinated or broken edges from the binary images (consider $n = \infty$, to remove the pixels that do not belong to the boundary so that it shrinks to a significantly connected stroke, and other portion with holes shrinks to a ring halfway between the outer boundary and the hole). Finally, the edges of the image are mixed by combining detected edges in the high-frequency as well as low-frequency portion.

The smaller value of $\varsigma_l$ would result in detecting more fine edges in the higher changes in intensity portion of the image. On the other hand, a higher value $\varsigma_h$ could detect edges in the lower change of intensity. A tradeoff could be achieved by choosing two different values of $\varsigma$, which is similar to the feature's synthesis step in the Canny edge detector. Thus, we have two different values of $\varsigma$, $\varsigma_h > \varsigma_l$ (through the

**Input:** Binary image: $b$ of size $m \times n$; Set of neighbor pixels $N = 4$, $\varsigma_l = 0.08$ *and* $\varsigma_h = 0.35$.
**Output:** Optimized edges: $oe$ of size $m \times n$; Set of operations to be executed $oe$.

if $\varsigma = \varsigma l$
  for all $\{i$ and $j \in \mathrm{N}\}$
    if $b_4\ (i, j) = 1$
      then $oe_l(i, j) = 0$;
    else $oe_l(i, j) = 1$;
  end if
end for
else if $\varsigma = \varsigma h$
  for all $\{i$ and $j \in N\}$
    if $b_4\ (i, j) = 1$
      then $oe_h\ (i, j) = 0$;
    else $oe_h\ (i, j) = 1$;
  end if
  end for
end if
then $oe = oe_l \cup oe_h$

Algorithm 1: Removal and cleaning of the isolated pixels and merging of detected edges.

experimental results for different values of $\varsigma$, we found that $\varsigma_l = 0.08$ and $\varsigma_h = 0.35$). Algorithm 1 merges the detected edges for higher and lower values of $\varsigma$; depending on the satisfaction of connectivity criteria, the edges are linked, which results in the direction of the majority of edges in the image.

## 4. Results Analysis

The FGTED technique is performed in Matlab-2023(a) with Intel(R) Core(TM) i3-3220 CPU @ 3.30 GHz, and it outperforms traditional approaches. The performance of the FGTED was carried out on the Berkeley Segmentation Dataset and Benchmark (BSDS 500), which is composed of 500 images that have manually annotated ground truth contours for each image. Edge detection accuracy is evaluated using six standard measures: structural similarity index measure (SSIM), *F*-score (*F*-measure), precision and recall (PR), signal-to-noise ratio (SNR), peak signal-to-noise ratio (PSNR), and computational time (CT).

The results are shown in Figure 2 for the images, which are randomly selected as experimental samples to compare it with the existing traditional approaches. Figure 2(a)–2(e) illustrates the comparative outcomes produced by several conventional techniques and the proposed FGTED on randomly selected images from BSD500. Figure 2(a) shows the ground truth image, Figure 2(b) shows the edges detected by the Prewitt edge detector, Figure 2(c) shows edges detected by the Sobel edge detector, Figure 2(d) shows the edges detected by Canny edge detector, and finally, Figure 2(e) shows edges detected by the FGTED.

From visual perceptions, Figure 2(e) presents better results than Figure 2(a)–2(d) for both the input images. The FGTED is capable of detecting very thin or microtype edges. The FGT value-based approach yielded a higher entropy image in comparison with the previously existing methods. The results of the statistical performance parameter are summarized and compared in Tables 1–6.

The visual comparison in Figure 2 also shows that the images depicted by the proposed edge detector are much better for the outer shape of the object than the other images obtained by the different existing edge detectors. The values of different parameters are shown in Tables 1–6, which also support the inferred results.

The output performance analysis of various images was also done using SSIM, *F*-score (*F*-measure), PR, SNR, PSNR, and CT, as shown in Tables 1–6. The achieved results are as follows:

(1) The SSIM, F-measure, SNR, and PSNR are better for FGTED for all the images shown in Tables 1, 2, 4, and 5. The result shows that FGTED performs better compared to all three edge detectors, viz. Prewitt, Sobel, and Canny.
(2) Results in Table 3 show the PR score, which is comparatively better than Prewitt and Sobel but lacking for some images compared to Canny, which can be further improved by adaptively changing the threshold as per need of the local region.
(3) Table 6 compares the total computation time of all the edge detectors, which also shows that the proposed edge detector is very fast compared to its other rivals.

This shows that the proposed FGTED detects the edges very fast, with significant improvement in the performance parameters compared to the other rival edge detectors.

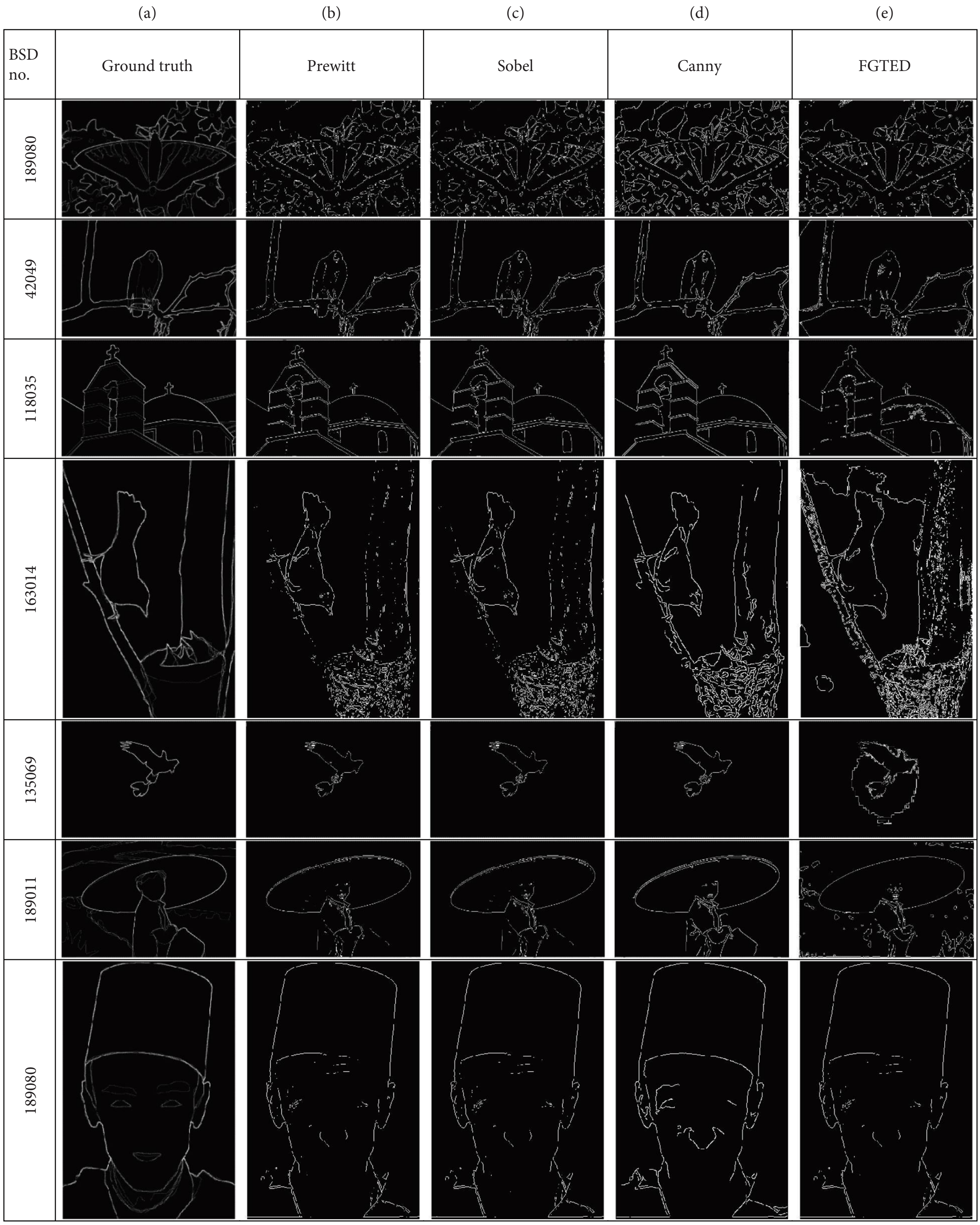


Figure 2: Experimental results using popular edge detectors and FGTED, where (a) ground truth images, (b) detected edges by the Prewitt edge detector, (c) detected edges by the Sobel edge detector, (d) detected edges by the Canny edge detector, (e) detected edges by FGTED.

Table 1: The statistical comparison for SSIM with the competitors on BSD500.

| | SSIM | | | |
|---|---|---|---|---|
| BSD image no. | Prewitt | Sobel | Canny | FGTED |
| 189080 | 0.504131 | 0.504158 | 0.504166 | 0.50419 |
| 42049 | 0.761943 | 0.762464 | 0.762506 | 0.762484 |
| 118035 | 0.741948 | 0.742701 | 0.742881 | 0.742713 |
| 163014 | 0.758939 | 0.75914 | 0.759262 | 0.759174 |
| 135069 | 0.944962 | 0.94487 | 0.944853 | 0.944872 |
| 189011 | 0.708242 | 0.708713 | 0.708748 | 0.708742 |
| 189080 | 0.791261 | 0.792347 | 0.792349 | 0.792357 |

Table 2: The statistical comparison for *F*-measure with the competitors on BSD500.

| | *F*-measure | | | |
|---|---|---|---|---|
| BSD image no. | Prewitt | Sobel | Canny | FGTED |
| 189080 | 0.008162 | 0.006528 | 0.005235 | 0.0069 |
| 42049 | 0.007377 | 0.004583 | 0.002448 | 0.004921 |
| 118035 | 0.00751 | 0.011472 | 0.011971 | 0.011988 |
| 163014 | 0.017671 | 0.007557 | 0.008561 | 0.008767 |
| 135069 | 0.013496 | 0.002132 | 0.002489 | 0.002131 |
| 189011 | 0.006133 | 0.00362 | 0.003774 | 0.003615 |
| 189080 | 0.007898 | 0.003522 | 0.001376 | 0.003809 |

Table 3: The statistical comparison for PR parameter with the competitors on BSD500.

| | PR parameter | | | |
|---|---|---|---|---|
| BSD image no. | Prewitt | Sobel | Canny | FGTED |
| 189080 | 12.07686 | 12.24877 | 15.72025 | 12.77581 |
| 42049 | 15.79185 | 15.83617 | 17.56378 | 15.77747 |
| 118035 | 11.18474 | 11.3226 | 13.3159 | 11.496811 |
| 163014 | 8.212761 | 8.638463 | 12.18637 | 14.13212 |
| 135069 | 15.08391 | 15.43197 | 18.56275 | 18.93553 |
| 189011 | 5.640497 | 5.693151 | 7.525693 | 5.812116 |
| 189080 | 7.694744 | 7.715008 | 9.937986 | 8.16019 |

Table 4: The statistical comparison for SNR parameter with the competitors on BSD500.

| | SNR (dB) | | | |
|---|---|---|---|---|
| BSD image no. | Prewitt | Sobel | Canny | FGTED |
| 189080 | −43.0911 | −43.4553 | −42.8961 | −43.3736 |
| 42049 | −44.5938 | −46.1048 | −45.3154 | −46.0563 |
| 118035 | −43.2846 | −43.0518 | −42.3015 | −43.0003 |
| 163014 | −40.2579 | −44.2129 | −43.3452 | −43.9134 |
| 135069 | −42.2813 | −46.5587 | −45.5488 | −46.4761 |
| 189011 | −42.0332 | −44.6548 | −44.3711 | −44.564 |
| 189080 | −40.7244 | −45.5497 | −45.1886 | −45.4726 |

Table 5: The statistical comparison for PSNR parameter with the competitors on BSD500.

| | PSNR (dB) | | | |
|---|---|---|---|---|
| BSD image no. | Prewitt | Sobel | Canny | FGTED |
| 189080 | 17.21255 | 17.21302 | 17.22229 | 17.21321 |
| 42049 | 17.97196 | 17.97413 | 17.98742 | 17.97416 |
| 118035 | 19.91756 | 19.91801 | 19.92993 | 19.91838 |
| 163014 | 18.78931 | 18.7844 | 18.78903 | 18.7848 |
| 135069 | 23.97576 | 23.97446 | 23.98405 | 23.97474 |
| 189011 | 20.67956 | 20.68491 | 20.69077 | 20.68498 |
| 189080 | 20.97487 | 20.97869 | 20.98875 | 20.97871 |

Table 6: The statistical comparison for computational time with the competitors on BSD500.

| | Time (s) | | | |
|---|---|---|---|---|
| BSD image no. | Prewitt | Sobel | Canny | FGTED |
| 189080 | 0.0504131 | 0.0504158 | 0.05282 | 0.025675 |
| 42049 | 0.0761943 | 0.0762464 | 0.01472 | 0.008680 |
| 118035 | 0.0741948 | 0.0742701 | 0.00896 | 0.010783 |
| 163014 | 0.0758939 | 0.075914 | 0.00804 | 0.007771 |
| 135069 | 0.0944962 | 0.094487 | 0.00784 | 0.005339 |
| 189011 | 0.0708242 | 0.0708713 | 0.00480 | 0.004217 |
| 189080 | 0.0791261 | 0.0792347 | 0.00691 | 0.007127 |

## 5. Conclusion

In this article, a novel FGTED is presented for computing microedges in minimum time without training or prior knowledge. It is concluded that Prewitt, Sobel, and Canny edge detectors eliminate very thin or microtype edges, while the proposed FGTED technique takes it into consideration. Figure 2(a)–2(d) shows the edges obtained by different classical edge detection techniques, whereas Figure 2(e) is the edge images detected by the FGTED. The FGTED technique exhibits better performance parameters for texture based images than the other prevailed methods. By the visual perceptions, the above results clearly indicate the superiority of the FGTED technique over the existing techniques. Hence, it is concluded that the FGTED works well for the detection of strong edges in comparison with the classical techniques. However, it is observed that the region near the hat-brim for BSD image no. 189,080 has broken edges, whereas for 135,069, it detected false edges around the birds. The scope of improvement is possible by applying local or adaptive thresholds using a fractional approach.

This technique gives improved results in minimum time, if intensity variations are correlated. Due to the fast speed for computing edges as well as fine outer boundary detection, this approach can be used in real-time applications where fast processing is required in object detection. The authors also suggest that the presented FGTED is a pathway for future innovations in FGT to get better edge detection for more digital images.

## Data Availability

No data were used to support this study.

## Conflicts of Interest

There are no conflicts of interest regarding the publication of this article.

## References


[1] A. A. Kilbas, H. M. Srivastava, and J. J. Trujiilo, *Theory and Applications of Fractional Differential Equations*, Elsevier, Amsterdam, 2006.

[2] A. C. McBride, "Fractional powers of a class of ordinary differential operators," *Proceedings of the London Mathematical Society*, vol. s3-45, no. 3, pp. 519–546, 1982.

[3] A. A. Kilbas and N. Sebastain, "Generalized fractional integration of Bessel function of first kind," *Integral Transforms and Special Functions*, vol. 19, no. 12, pp. 869–883, 2008.

[4] V. Kiryakova, "A brief story about the operators of the generalized fractional calculus," *Fractional Calculus and Applied Analysis*, vol. 11, no. 2, pp. 203–220, 2008.

[5] D. Baleanu, K. Diethelm, E. Scalas, and J. J. Trujillo, *Fractional Calculus Models and Numerical Methods, Series on Complexity, Nonlinearity and Chaos*, World Scientific, 2012.

[6] B. C. Gaur Sanjay, S. Mehta, and J. Vajpai, "Adaptive local thresholding for edge detection," *International Journal of Computer Applications*, pp. 15–18, 2014.

[7] B. C. Gaur Sanjay and J. Vajpai, "An innovative fuzzy logic based approach for edge detection," *International Journal Of Engineering Research & Technology (Ijert) Etrasct*, vol. 2, no. 3, 2014.

[8] J. M. Blackledge, *Diffusion and Fractional Diffusion Based Image Processing*, pp. 233–240, EG UK Theory and Practice of Computer Graphics, 2009.

[9] B. Mathieu, P. Melchior, A. Oustaloup, and C. Ceyral, "Fractional differentiation for edge detection," *Signal Processing*, vol. 83, no. 11, pp. 2421–2432, 2003.

[10] J. You, S. Hungnahally, and A. Sattar, "Fractional discrimination for texture image segmentation," *International Conference on Image Processing*, vol. 1, pp. 220–223, 1997.

[11] J. Canny, "A computational approach to edge detection," *IEEE Transactions on Pattern Analysis and Machine Intelligence*, vol. PAMI-8, no. 6, pp. 679–698, 1986.

[12] H. Jeong and C. I. Kim, "Adaptive determination of filter scales for edge detection," *IEEE Transactions on Pattern Analysis and Machine Intelligence*, vol. 14, no. 5, pp. 579–585, 1992.

[13] R. C. Gonzalez and R. E. Woods, *Digital Image Processing*, pp. 692–794, Prentice Hall, 3rd edition, 2013.

[14] M. B. Ahmad and T.-S. Choi, "Local threshold and Boolean function based edge detection," *IEEE Transactions on Consumer Electronics*, vol. 45, no. 3, pp. 674–679, 1999.

[15] M. Basu, "Gaussian-based edge-detection methods—a survey," *IEEE Transactions on Systems, Man and Cybernetics, Part C (Applications and Reviews)*, vol. 32, no. 3, pp. 252–260, 2002.

[16] S. B. C. Gaur and J. Vajpai, "Comparison of edge detection techniques for segmenting car license plates," *Special Issue of International Journal of Computer Applications on Electronics, Information and Communication Engineering*, vol. 5, pp. 8–12, 2011.

[17] Y.-F. Pu, J.-L. Zhou, and X. Yuan, "Fractional differential mask: a fractional differential-based approach for multiscale texture enhancement," *IEEE Transactions on Image Processing*, vol. 19, no. 2, pp. 491–511, 2010.

[18] K. Diethelm, N. J. Ford, and A. D. Freed, "A predictor–corrector approach for the numerical solution of fractional differential equations," *Nonlinear Dynamics*, vol. 29, no. 1/4, pp. 3–22, 2002.

[19] M. Z. Sarikaya and H. Yaldiz, "On hermite-hadamard type inequalities for $\varphi$-convex functions via fractional integrals," *Malaysian Journal of Mathematical Sciences*, vol. 9, no. 2, pp. 243–258, 2015.

[20] S. K. Ntouyas, P. Agarwal, and T. Jessada, "On Polya-Szegö and Chebyshev types inequalities involving the Riemann–Liouville fractional integral operators," *Journal of Mathematical Inequalities*, vol. 10, no. 2, pp. 491–504, 2016.

[21] A. Khmag, A. R. Ramli, and N. Kamarudin, "Clustering-based natural image denoising using dictionary learning approach in wavelet domain," *Soft Computing*, vol. 23, no. 17, pp. 8013–8027, 2019.

[22] A. Khmag, "Additive Gaussian noise removal based on generative adversarial network model and semi-soft thresholding approach," *Multimedia Tools and Applications*, vol. 82, no. 5, pp. 7757–7777, 2023.

[23] Khmag and N. Kamarudin, "Natural image deblurring using recursive deep convolutional neural network (R-DbCNN) and second-generation wavelets," in *2019 IEEE International Conference on Signal and Image Processing Applications (ICSIPA)*, pp. 285–290, IEEE, Kuala Lumpur, Malaysia, 2019.

[24] D. Martin, C. Fowlkes, D. Tal, and J. Malik, "A database of human segmented natural images and its application to evaluating segmentation algorithms and measuring ecological statistics," *Proceedings of the IEEE International Conference on Computer Vision*, vol. 2, pp. 416–423, 2001.

[25] A. Nandal, H. Gamboa-Rosales, A. Dhaka et al., "Image edge detection using fractional calculus with feature and contrast enhancement," *Circuits, Systems, and Signal Processing*, vol. 37, no. 9, pp. 3946–3972, 2018.